Stretchable Optical Waveguide Sensor Suitability for Wrinkle Degree Detection in Soft Robots

J. Garrett Williamson[1] and Joshua Schultz[1]

***Abstract*— Optical waveguide deformation sensors are created for less than 15 US Dollars each and evaluated for their usefulness in detecting the severity of wrinkles in a thin-walled soft robot. This severity is quantified by the bend angle produced in the robot. The sensors are integrated into the skin of the robot and tests are performed to determine their usefulness. The sensors prove to be able to accurately track the bend angle of the robotic arm as a wrinkle is induced in a sudden load drop test, a sudden pressure loss test, an incremented load test, and an incremented pressure test. The drop test, specifically, tracked bend angle through many rapid undulations.**

I. INTRODUCTION

As the field of soft robotics has developed, one of the key abilities researchers have proposed for them is that of navigating unstructured environments better than their hard counterparts. While this ability has often been touted [1]–[4], it has yet to be fully realized. One major obstacle on the path toward soft robots that easily navigate their environment is wrinkling. For this work, the term wrinkling comes from inflated beam theory. It can be loosely defined as the region beyond the point when longitudinal stress from inflation reaches equilibrium with the stress induced by some bending moment [5]–[7]. In this region, wrinkles form at the base of the beam and become more and more severe until total collapse occurs. The detection and modeling of wrinkles that form as a soft robot is loaded or encounters an obstacle is essential to performing tasks in an unstructured environment. As of yet, this aspect of soft robotics has gone largely unstudied. One work in 2019 did seek to address this question [8]. However, the robot they used for testing was reinforced with a metal spring, which prevented extremely high local curvatures from occurring. These wrinkles occur frequently with our group's single-chambered, thin-walled soft robot: Squishy [9], [10]. While one may think that this is a disadvantage of thin-walled robots, there are instances in which wrinkling may be useful in performing a task. One could imagine a similar situation to Figure 1 in which a robot seeks to lower an object over a ledge. Another instance may be the need to purposefully induce a wrinkle so that a robot can wrap back on itself to turn around in a tunnel. A soft robot's ability to wrinkle sets it apart from hard robots and that ability should be taken advantage of.

This work is supported by the NSF grant No. 1935312 EFRI C3 SoRo: Between a Soft Robot and a Hard Place: Estimation and Control Algorithms that Exploit Soft Robots' Unique Abilities

[1]J. Garrett Williamson (student member IEEE) and Joshua Schultz (senior member IEEE) are with the Department of Mechanical Engineering, University of Tulsa, 800 S Tucker Dr, Tulsa, OK 74104, The United States jgw3642@utulsa.edu, joshua-schultz@utulsa.edu

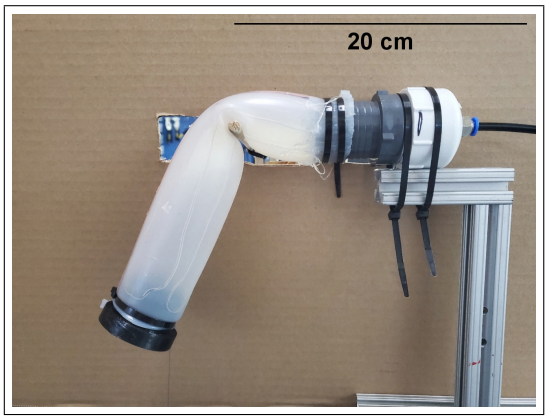

Fig. 1. Wrinkle of High Local Curvature Induced in Squishy by a Load and Dowel Rod Fulcrum

Wrinkles present two challenges to knowing a soft robot's configuration. These are modeling and sensing. The two most popular models in soft robotics currently are the Kirchoff/Cosserat rod model [11], [12] and the piecewise constant curvature model [13], [14]. The Kirchoff/Cosserat rod and piecewise constant curvature models trade-off between model fidelity on the Kirchoff/Cosserat rod side and simplicity on the piecewise constant curvature side. Both of these types of models, however, are based on the assumption that there is constant curvature and differentiability between each of the discrete sections. This means that, while they can in theory deal with high localized curvature, to do so requires a high degree of discretization to ensure that the location where the wrinkle occurs will have a small enough segment to capture the large local curvature. One promising model under development that may be able to represent the high local curvatures is that of the Disc Thread model [9], but this model will require an accurate location and severity of wrinkle to determine the robot's new configuration.

This study seeks to address the challenge of sensing the presence and severity of wrinkles. Furthermore, it would be desirable for whatever sensor is used for wrinkle detection to also detect other modes of deformation. The stretchable optical waveguides of Harnett et al. posses this multi-modality and other desirable characteristics [15]. These sensors show sensitivity, not only to the bending that would be introduced by a wrinkle but also to locally applied pressure and longitudinal strain. Harnett et al., only investigated longitudinal strain in the sensor they built; however, a very similar sensor was previously investigated for all three modes (bending, longitudinal strain, and locally applied pressure) by Zhao et

2023 IEEE International Conference on Soft Robotics (RoboSoft) | 979-8-3503-3222-3/23/$31.00 ©2023 IEEE | DOI: 10.1109/ROBOSOFT55895.2023.10122087

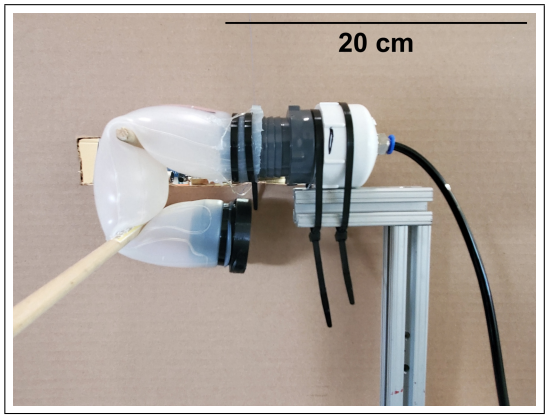

Fig. 2. Squishy Exhibiting Wrinkles in Two Locations

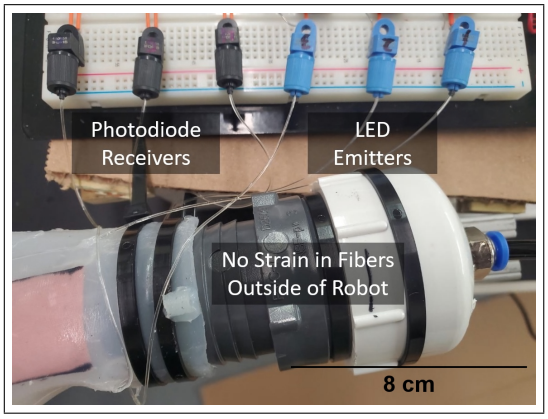

Fig. 3. Sensor Connections

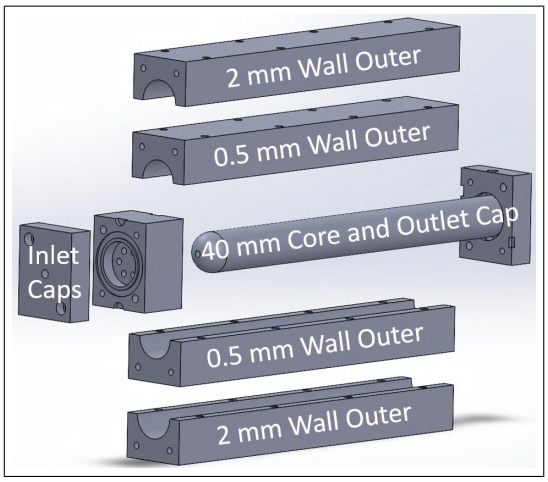

Fig. 4. Machined Aluminum Mold Assembly

al. [16].

The overall work of our research group involves single-chambered soft robots with relatively thin walls with some fabric reinforcement [9], [10]. Because of this, it was necessary to incorporate these sensors into the walls of one of these soft robots.

II. SENSING

Stretchable light waveguide sensors are not new, though their application to soft robotics is [15]–[18]. They rely on the same principle as fiber optics, though they do not achieve the same total internal reflectivity. For sensing, this is actually desirable, as the loss in light intensity due to deformation is an indicator of how much the fiber has bent. Aside from the multimodal sensing capability mentioned earlier, another reason for choosing these sensors for this project is that they are not interfered with by electric or magnetic fields [19]. This is useful for robots that move by selectively stiffening their walls using magnetorheological or electrorheological fluids [9], [10], [20].

In some applications, soft robots may wrinkle or pleat in more than one location. If this occurs, there may be more than one wrinkle crossing an individual waveguide. Ideally, such a sensor would be able to detect this superposition of wrinkles along this length. That is, if the sensor is bent at some point along its path as in Figure 1, then bent to an equal degree further along that path, as seen in Figure 2, the signal change from the addition of the second bend is of similar amplitude to the first, or at least it is detectable.

III. MANFACTURING

As in Harnett et al. we use a commercially available polyurethane core of 0.8 mm in diameter called Stretch Magic^{TM}. However, the robots our group has been working with are made from the Dragon Skin^{TM} series of silicones from Smooth-On, Inc. In the work of Harnett et al., the polyurethane fiber is clad with Elastosil M 4641. It was found, however, that the polyurethane fiber guides light sufficiently well clad in Dragon Skin 10 for sensing and also guides well with no cladding at all once the sensor exits the robot, though the latter observation was also noted by Harnett et al. Industrial Fiber Optics IF-E91A, 935 nm LEDs were used as the emitters and IF-D91B photodiodes were used as the receivers (Figure 3). These components are made to receive 2.2 mm jacketed plastic fiber optic cable and cannot clamp onto the 0.8 mm polyurethane fiber. Therefore, two layers of heat shrink were applied to each end of the fiber to increase its diameter. Because the fibers are being incorporated into the skin of the robot, the only strain present exists within that skin and not on the coupling between those fibers and their emitters or receivers (see Figure 3), which prevents the fiber from pulling out of the heat shrink or photodiode/LED.

Since the chosen fiber diameter was 0.8 mm and the robot's walls are 2 mm thick, the 3D-printed mold tolerances from our previous work were insufficient [10]. In order to locate the fiber in the center of the wall, a two-part machined metal mold was designed. The first part of this mold creates a 0.5 mm thick skin of Dragon Skin 10^{TM} elastomer. Sensors and fabric are then adhered to this skin using Sil-Poxy^{TM}. The final 1.5 mm of the skin is then molded over the 0.5 mm skin, fabric, and adhered sensors (see Figure 5).

The machined metal mold used in this process consists of a 40 mm diameter bar of 440C stainless steel rotary shaft press-fit into an end cap with two outflow ports as seen in

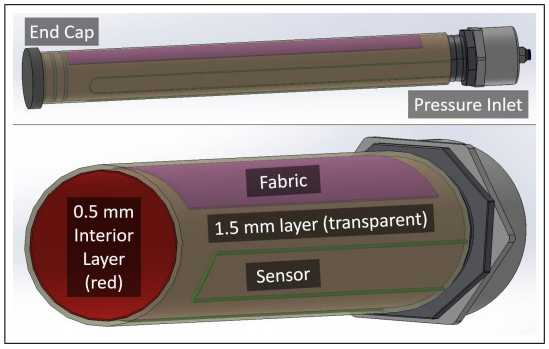

Fig. 5. Completed Robot and its Various Component Placements

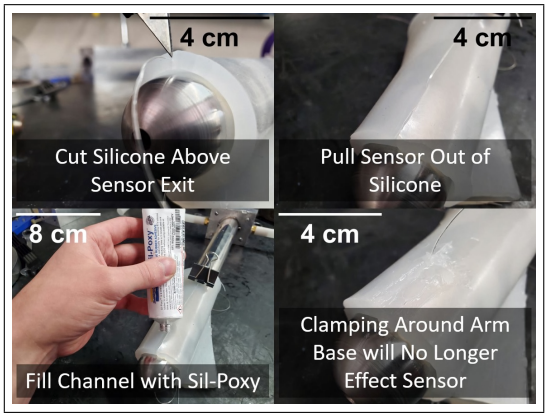

Fig. 6. Lead Removal Process (6 mm Thick Skin for Clarity)

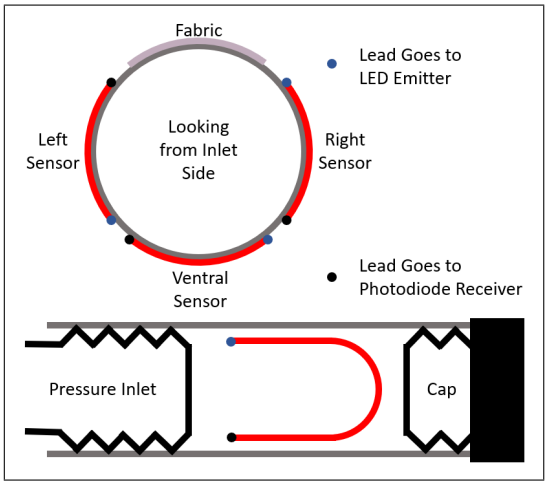

Fig. 7. Sensor Placement

Figure 4. This end cap and the rest of the mold are machined with a HAAS CNC out of 6061 aluminum stock. Two outer shells are bolted together and slide over the bar. They are held in place to the end cap with two pins and two bolts. This assembly is then capped by a block containing six spaced-out holes to ensure that the silicone spreads out evenly upon injection. This is aligned to the outers with two pins. Another cap with one input port slides over another set of two pins to align to that cap. The two inlet caps are then bolted through to the outers. The split cap design helps in cleaning. Sealing is assured with two o-rings; one between the inlet caps and one between the inlet cap and the outers. Sealing between the outers is accomplished by polishing their interface with lapping paper up to 2000 grit and covering that interface with vacuum grease. Sealing where the outlet cap meets the outers was neglected as it could not introduce air into the body of the robot.

This assembly is placed with the input port down and disposable tubing connected to that port. This tubing is subsequently connected to a silicone reservoir funnel. The two outflow ports are connected to a vacuum pump through a catch pot. The catch pot prevents silicone from inadvertently entering the vacuum pump. This mold has an estimated precision of 0.0381 mm and creates soft robots with very uniform wall thicknesses. This is important both for positioning sensors accurately and preventing wall rupture. In the experience of this team, non-uniform walls are the primary culprit behind a soft robot bursting.

Once all of this is attached, the silicone reservoir is filled with Dragon Skin 10^{TM} SLOW that has been pre-degassed and the mold is subjected to vacuum. The orientation means that silicone is drawn up by the vacuum from bottom to top. This and a vacuum's ability to degas silicone ensures there are no voids in the final product. Once the silicone for the first 0.5 mm thick stage is cured, three sensors and a strip of fabric were placed on that skin such that they formed the up, down, left, and right quarters of the robot's skin, as shown in Figures 5 and 7, and adhered with Sil-Poxy^{TM}. After which, the mold outer shells are swapped to create a 2 mm skin and the pouring process is repeated.

After the silicone has cured, the mold is opened and the sprues and other excess silicone are cut away from the top and bottom to leave a tube of silicone with incorporated sensors and fabric. Care must be taken when trimming the silicone from the bottom of the robot to ensure no sensor leads are cut. The outer layer of silicone above the sensor is also cut for about 8 cm and the resulting cavity is filled with Sil-Poxy^{TM}. This results in the sensor leads leaving the robot distal to the barbs of the pressure inlet as shown in Figures 6 and 7. This is to prevent the clamping force and local deformations at the barb from influencing the sensor signal. If the strand passes the barb at the base of the robot, losses due to this clamping force obscure the bending of the robot itself.

IV. MATERIALS AND METHODS

The tests were run with a power supply powering each LED and an oscilloscope sampling at 5 kHz on each photodiode to monitor the voltage it produced when light induced a current over its internal resistance. This data was then digitally filtered with a moving mean filter set to average over 500 samples. The true bend angle of the wrinkle was calculated from two motion-tracking sensors connected to a Polhemus Liberty motion-tracking system. One was used as a reference while the other tracked the tip as seen in Figure 9. Chamber pressure was also monitored during each test.

TABLE I
TEST CONDITIONS

	Drop Test	Incremented Pressure Test	Incremented Weight Test	Simulated Rupture Test
Weight (grams)	210	110	50-210	110
Pressure (kPa)	8.58	9.65-5.4	8.58	9.65

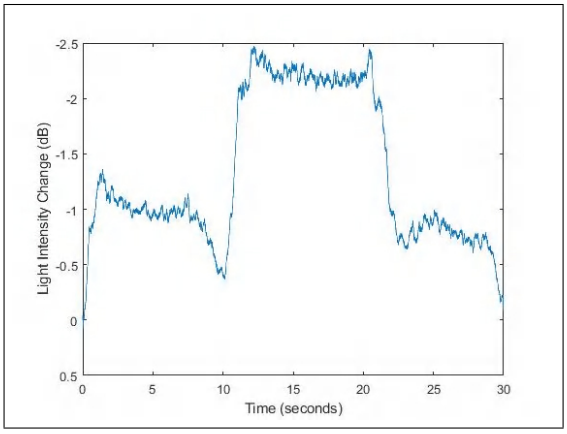

Fig. 8. Double Bend Sensor Measurement

The weight set used for all tests can also be seen in Figure 9, as can the dowel rod used as an environmental obstacle.

The first test conducted was the drop test. It involved the sudden application of a 210-gram load for an arm at a pressure of 8.58 kPa. The weight was then quickly lifted back up once the robot had stopped undulating. The next test involved decreasing pressure from 9.65 kPa and 5.4 kPa then returning it to 9.65 kPa with the arm bearing a 110-gram load. The incremented weight test started with a 50-gram load and successively added 20 grams at a time up to 210 grams then removed it in the same manner. This test was conducted at a pressure of 8.58 kPa. The simulated rupture test loaded the arm with a 110-gram load. The pressure was suddenly dropped from 9.65 kPa to 0 and returned to the same pressure once the arm stopped undulating. A summary of the tests conducted can be seen in Table I. These tests were performed for four orientations in which each side (fabric, left sensor, right sensor, and ventral sensor) was facing toward the dowel rod.

V. RESULTS AND DISCUSSION

While most sensors, including these, can reach a saturation limit, they do appear to have the desired superposition characteristic mentioned previously as seen in Figure 8. The first plateau denotes the loss in intensity due to the initial bend as seen in Figure 1. The second plateau denotes the same, but for the second bend as seen in Figure 2. The third is the return to the first, single-bend configuration.

It can be seen in Figures 10, 11, and 12 that the profile of the sensor measurement follows the profile measured by the external Polhemus Liberty sensors for each of the test types, up to a multiplicative constant, which can be determined by

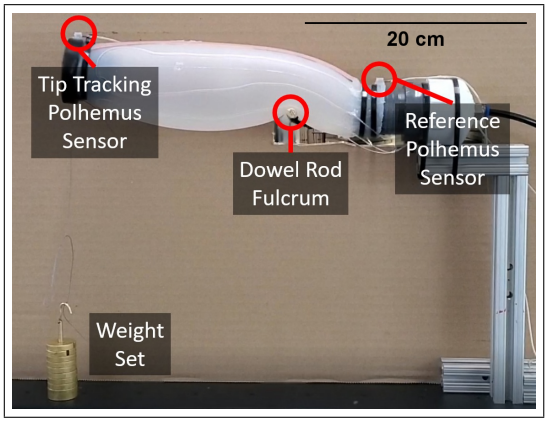

Fig. 9. Starting Position for Drop Test

a calibration routine. In fact, though the application of each weight in the incremented weight test was done in such a way as to minimize undulation, the sensor captures the stepping, damped-sinusoid behavior as seen in Figure 12. Each stair step represents the application of the next weight.

Examining the curves and especially Figure 10, there is no visible lag between the Polhemus and the sensor on the timescale shown. The reference and sensor data for these tests were externally synced. This indicates that the sensors have sufficient bandwidth to reconstruct the configuration even during highly dynamic motions where the robot develops wrinkles as it oscillates at its natural mechanical frequencies.

It should be noted that in the locations in these fabric-up tests where the sensor curve does deviate from the ground-truth bend angle, it is close to a bend angle of less than 5 degrees or greater than 25. This may be due to the sensor nearing either its minimum or maximum useful limits. For the lower limit, it should be noted that in the work of Harnett et al., a similar need to pre-strain sensors was discovered. This would explain the tendency for the sensor to not start following the bend angle until it reaches a limit. This would cause the truncation of the curves observed in all the tests. The upper limit (saturation) behavior can be observed in Figures 12 and 13. In these tests, the sensor curve deviates from the ground-truth bend angle. This is especially true for the simulated rupture test of Figure 13. This test had the greatest bend angle as the chamber was allowed to completely deflate and also showed the worst deviation from the true bend angle. This may be due to an observed tendency for the sensor to carry more light as it approaches saturation or the stick-slip motions of the fiber within the channel.

An additional attribute of these sensors is their low cost. Each sensor costs less than 15 US dollars to create, including its electronic components.

A. Limitations

During tests, it was noted that the unloaded arm does not curve as far toward the fabric as in tests without the incorporated sensors. This is due to polyurethane being stiffer than Dragon Skin 10^{TM}. Another observation was that the

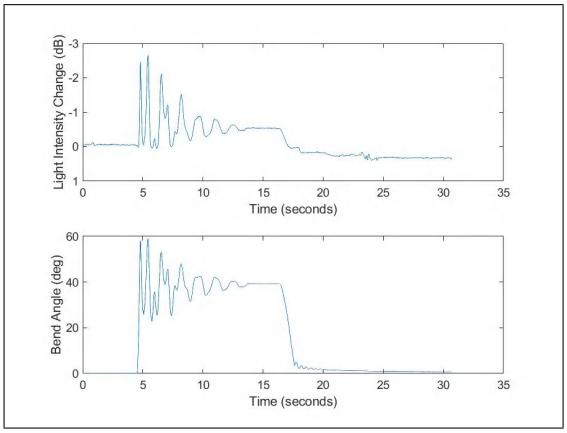

Fig. 10. Drop Test with Fabric Facing Upward

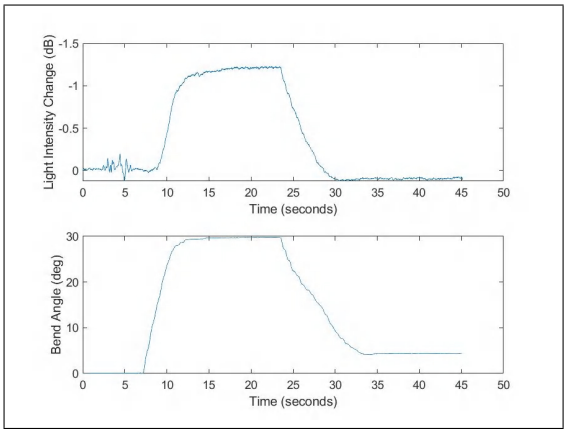

Fig. 11. Incremented Pressure Test with Fabric Facing Upward

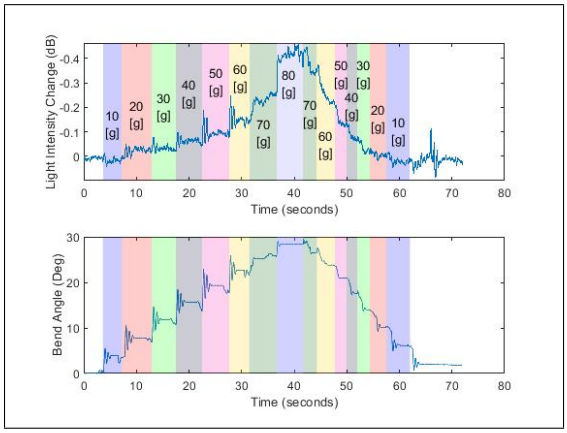

Fig. 12. Incremented Weight Test with Fabric Facing Upward

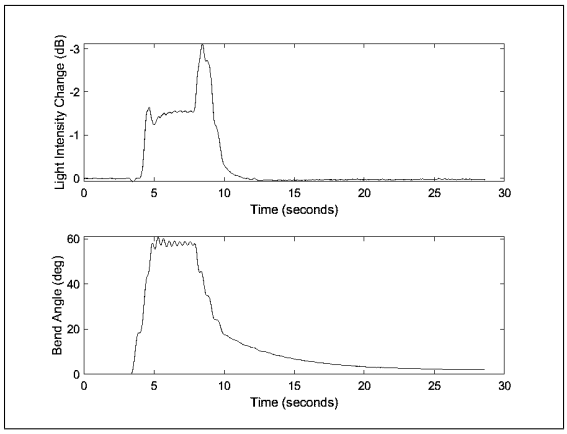

Fig. 13. Simulated Rupture Test with Fabric Facing Upward

polyurethane sensors did not adhere well within the skin of the robot, which may have caused the previously proposed stick-slip behavior. As the skin deformed under inflation and load, the sensor could slide along the channel within the wall. While this would cause difficulty in locating one or more wrinkles along the body of the robot, it did not seem to largely affect the sensors' ability to accurately determine the degree of the wrinkle over time in most tests.

Another issue noted was the high degree of variability between sensors. For the four types of tests performed on the four different sides, the left sensor was consistently more sensitive as it carried more light than the other sensors in the undeformed state. Sensor variability made the data from all tests other than the one in which the fabric was facing upwards inconsistent. Part of this was due to the fact that whichever sensor was placed directly on the dowel rod saturated from the locally applied pressure and produced no usable signal.

An additional consideration mentioned in the introduction is the multi-modal nature of these sensors. They detect bending, locally applied pressure, and longitudinal strain as demonstrated by Zhao et al. [16]. We confirmed this by some rudimentary local pressure tests using weights and bending tests using cylinders of known radii. While it is believed that the coupled nature of these sensors can be a strength when they are used in large numbers and in conjunction with other sensor data like pressure, it makes decoupling the three sensed modes difficult. This means that determining bend angle from the sensor data alone across all test types and orientations, is not currently possible. The purpose of this study was to determine whether these sensors showed promise for use in wrinkle detection. The results indicate that they do, but stick-slip behavior, manufacturing variability, and deformation mode decoupling will all have to be addressed before they can realize their proposed potential.

VI. CONCLUSIONS

In this study, optical waveguide sensors were evaluated for their usefulness in detecting and classifying wrinkles induced in a thin-walled soft robot by the bend angle which they produce. Three of these 0.8 mm diameter sensors were incorporated into the 2 mm thick wall of a fabric-reinforced robot using a high-precision machined metal mold. This robot was then tested by inducing wrinkles using a suddenly applied load, a sudden decrease in pressure, an incrementally increased load, and incrementally decreased pressure. Though deviations were noted around the upper and lower limits of the sensor's range, the sensor curves closely matched the ground truth bend angle curves.

Stretchable light waveguide sensors show promise for detecting the severity of a wrinkle by quantifying the bend angle it induces, but they are very sensitive to things like locally applied pressure and jostling. They have high bandwidth and, when properly made and connected, can very accurately track the bend angle of the robot about its fulcrum. Given this sensor type's ability to track longitudinal strain, locally applied pressure, and bend angle, they should also be useful in perception to determine the robot's configuration when there isn't a wrinkle.

While polyurethane fiber is not perfectly suited for this application, because of its higher shore hardness and lack of adhesion to silicone, to the authors' knowledge, optically clear, small-diameter, low-shore hardness, silicone fibers of sufficient length are neither commercially available nor have been produced in a lab. Because the field of soft robotics already suffers from few useful commercially available sensors, seeking to use off-the-shelf materials whenever possible benefits the community as a whole.

Moving forward, the first task will be to fine-tune these sensors. Creating a better way to connect them to their emitters and receivers would likely help with the variability seen between sensors. While the benefits of using commercially available supplies have already been mentioned, it is difficult to verify the optical and mechanical uniformities of Stretch Magic™. It would also be useful to change from polyurethane to silicone as in Guo et Al. so that they bond with the skin rather than just sliding within it [18]. However, the sensors created by Guo et Al. were 4 centimeters long, while the sensors needed for our application must be around 1 meter long.

Additionally, a better arm manufacturing system should be created. While the first mold and pouring setup was able to produce arms with high-tolerance skin thicknesses, it had some difficulties. First, the need for the outers to slide along the pins on the outlet cap before they can be unbolted and pulled away in the perpendicular direction to the bar, causes the 0.5 mm skin to wrinkle sometimes. Also, using gasket material instead of a polished, vacuum-greased interface between the outers would help in achieving a better seal. An additional o-ring added to the outlet cap would also help with this. The reason for seeking to achieve a higher degree of sealing is that, occasionally, the 0.5 mm skin stops partway up the mold. Another change that may help with this would be to apply pressure at the funnel to help push the silicone in addition to the vacuum pulling it.

After the sensors themselves are made more consistent, the next task will be to optimize sensor placement not only for both wrinkle detection and locating, but also for returning the most useful perceptual information aside from the location and severity of a wrinkle. Once this is done, the data from these sensors must be decoupled into wrinkle location and degree and other strain modes like longitudinal and locally applied pressure. To accomplish this, it may be necessary to train a simple neural network. After decoupling the strain modes, this data can be incorporated along with dynamic models for Soft Robot planning and control.

ACKNOWLEDGMENT

The authors would like to acknowledge the contributions of Dustin Donnell and Christifer Lee of the University of Tulsa McElroy Prototyping Lab. Their aid in the design and fabrication of the high-precision machined metal mold detailed in this paper is greatly appreciated.

REFERENCES

[1] D. Drotman, S. Jadhav, M. Karimi, P. de Zonia, and M. T. Tolley, "3d printed soft actuators for a legged robot capable of navigating unstructured terrain," in *2017 IEEE International Conference on Robotics and Automation (ICRA)*, pp. 5532–5538, 2017.

[2] S. Kim, C. Laschi, and B. Trimmer, "Soft robotics: a bioinspired evolution in robotics," *Trends in biotechnology*, vol. 31, no. 5, pp. 287–294, 2013.

[3] D. Trivedi, C. D. Rahn, W. M. Kier, and I. D. Walker, "Soft robotics: Biological inspiration, state of the art, and future research," *Applied bionics and biomechanics*, vol. 5, no. 3, pp. 99–117, 2008.

[4] C. D. Santina, R. K. Katzschmann, A. Bicchi, and D. Rus, "Model-based dynamic feedback control of a planar soft robot: trajectory tracking and interaction with the environment," *The International Journal of Robotics Research*, vol. 39, no. 4, pp. 490–513, 2020.

[5] S. Veldman, O. Bergsma, and A. Beukers, "Bending of anisotropic inflated cylindrical beams," *Thin-walled structures*, vol. 43, no. 3, pp. 461–475, 2005.

[6] J. A. Main, S. W. Peterson, and A. M. Strauss, "Beam-type bending of space-based inflated membrane structures," *Journal of Aerospace Engineering*, vol. 8, no. 2, pp. 120–125, 1995.

[7] S. L. Veldman, *Design and analysis methodologies for inflated beams*. 2005.

[8] L. Pan, P. Yao, Y. zhang, and G. Bao, "Bending and wrinkled model research of a soft robot inspired by octopus," in *2018 3rd International Conference on Advanced Robotics and Mechatronics (ICARM)*, pp. 726–731, 2018.

[9] J. A. Schultz, H. Sanders, P. D. H. Bui, B. Layer, and M. Killpack, "Modeling the dynamics of soft robots by discs and threads," in *2022 International Conference on Robotics and Automation (ICRA)*, pp. 3223–3229, 2022.

[10] J. G. Williamson, C. Schell, M. Keller, and J. Schultz, "Extending the reach of single-chamber inflatable soft robots using magnetorheological fluids," in *2021 IEEE 4th International Conference on Soft Robotics (RoboSoft)*, pp. 119–125, 2021.

[11] F. Renda, F. Boyer, J. Dias, and L. Seneviratne, "Discrete cosserat approach for multisection soft manipulator dynamics," *IEEE Transactions on Robotics*, vol. 34, no. 6, pp. 1518–1533, 2018.

[12] D. C. Rucker and R. J. Webster III, "Statics and dynamics of continuum robots with general tendon routing and external loading," *IEEE Transactions on Robotics*, vol. 27, no. 6, pp. 1033–1044, 2011.

[13] A. D. Marchese and D. Rus, "Design, kinematics, and control of a soft spatial fluidic elastomer manipulator," *The International Journal of Robotics Research*, vol. 35, no. 7, pp. 840–869, 2016.

[14] S. Neppalli, M. A. Csencsits, B. A. Jones, and I. D. Walker, "Closed-form inverse kinematics for continuum manipulators," *Advanced Robotics*, vol. 23, no. 15, pp. 2077–2091, 2009.

[15] C. K. Harnett, H. Zhao, and R. F. Shepherd, "Stretchable optical fibers: Threads for strain-sensitive textiles," *Advanced Materials Technologies*, vol. 2, no. 9, p. 1700087, 2017.

[16] H. Zhao, K. O'Brien, S. Li, and R. F. Shepherd, "Optoelectronically innervated soft prosthetic hand via stretchable optical waveguides," *Science Robotics*, vol. 1, no. 1, p. eaai7529, 2016.

[17] J. Missinne, S. Kalathimekkad, B. V. Hoe, E. Bosman, J. Vanfleteren, and G. V. Steenberge, "Stretchable optical waveguides," *Opt. Express*, vol. 22, pp. 4168–4179, Feb 2014.

[18] J. Guo, M. Niu, and C. Yang, "Highly flexible and stretchable optical strain sensing for human motion detection," *Optica*, vol. 4, pp. 1285–1288, Oct 2017.

[19] H. Wang, M. Totaro, and L. Beccai, "Toward perceptive soft robots: Progress and challenges," *Advanced Science*, vol. 5, no. 9, p. 1800541, 2018.

[20] K. J. McDonald, L. Kinnicutt, A. M. Moran, and T. Ranzani, "Modulation of Magnetorheological Fluid Flow in Soft Robots Using Electropermanent Magnets," *IEEE Robotics and Automation Letters*, vol. 7, no. 2, pp. 3914–3921, 2022.